TABLE 2 Comparison of Measured Half-Power Beamwidth in *E*- and *H*-Planes and Front-to-Back Ratios at 1.8, 2.35, and 2.6 GHz

	E-plane				*H*-plane			
	HPBW (°)		FBR (dB)		HPBW (°)		FBR (dB)	
Freq. (GHz)	STDA	Proposed	STDA	Proposed	STDA	Proposed	STDA	Proposed
1.8	71	57	13.0	14.4	116	111	12.9	17.7
2.35	67	76	13.1	16.6	111	115	14.7	16.9
2.6	68	78	12.5	13.2	106	105	13.3	14.2

4. EXPERIMENTAL RESULTS AND DISCUSSION

A conventional STDA antenna [9] and a proposed compact STDA antenna with top loading, as shown in Figure 1(b), are fabricated on an FR4 substrate, and their performance characteristics are compared. Figure 5 shows the photographs of the fabricated antennas.

Figure 6 presents the simulated and measured input VSWR and realized gain characteristics of the fabricated STDA and proposed antennas. The bandwidths of the STDA and proposed antennas for a VSWR < 2 are about 47.3% (1.68–2.72 GHz) and 48.0% (1.68–2.74 GHz), respectively, for the simulation, and about 47.8% (1.72–2.80 GHz) and 48.7% (1.68–2.76 GHz), respectively, for the measurement. In the band from 1.7 to 2.6 GHz, the measured gains of the STDA and proposed antennas are 5.5–6.2 and 5.6–6.0 dBi, respectively. The realized gain of the proposed antenna is improved at a low operating frequency band, but is slightly decreased or stays almost the same in the remaining frequencies. From these comparison results, we can conclude that the proposed antenna with a lateral size reduction of 14.3% shows similar performance with minimal degradation compared to the conventional STDA antenna.

The radiation patterns of the fabricated STDA and proposed antennas in the *E*-plane(*x*-*y* plane) and *H*-plane(*y*-*z* plane) at 1.8, 2.35, and 2.6 GHz are plotted in Figure 7.

Table 2 summarizes the measured half-power beamwidth in the *E*- and *H*-planes and the FBR at 1.8, 2.35, and 2.6 GHz. We see from Table 2 that the FBR of the proposed antenna is 13.2–17.7 dB, which is 0.7 to 4.8 dB better than those of the STDA antenna.

5. CONCLUSION

We have presented the design of a compact broadband STDA antenna with top loading for size reduction. To reduce the lateral size of a conventional STDA antenna, rectangular patch-shaped top loading is used for the two dipole elements, and a grooved ground plane is used by adding a patch at both ends of the ground plane. The effects of varying the length and width of the rectangular patch-shaped top loading on the antenna performances are investigated. A proposed STDA antenna covering a frequency band ranging from 1.7 to 2.7 GHz with a gain > 5 dBi is designed with the total antenna width reduced by approximately 14.3% compared to the STDA, but a little degradation in the antenna performances.

To validate the proposed design method, an STDA antenna and a proposed compact STDA antenna with top loading are fabricated on an FR4 substrate. Experimental results show that the proposed compact antenna presents a 48.7% bandwidth in the range of 1.68–2.76 GHz and a stable gain of 5.6–6.0 dBi with minimal degradation. Moreover, the FBR is improved by about 0.7 to 4.8 dB.

The proposed broadband STDA antenna can be used as antennas for low-power (indoor) repeaters integrating various mobile communication systems (PCS, IMT-2000, LTE) and wireless services (WiBro, WLAN, Bluetooth, WiMAX), or as an element antenna of a wideband high-gain base-station antenna for mobile communications.

REFERENCES

1. R. Waterhouse, Printed antennas for wireless communications, Wiley, England, 2007.
2. F. Tefiku and C.A. Grimes, Design of broad-band and dual-band antennas comprised of series-fed printed-strip dipole pairs, IEEE Trans Antennas Propag 48 (2000), 895–900.
3. A.A. Eldek, Design of double dipole antenna with enhanced usable bandwidth for wideband phased array applications, Prog Electromagn Res 59 (2006), 1–15.
4. G. Kumar and K.P. Ray, Broadband microstrip antennas, Artech House, Norwood, MA, 2003.
5. W. Baixiao, C. Aixin, and S. Donglin, An improved fractal tree log periodic dipole antenna, Proceedings 19th APEMC, 2008, pp. 831–834.
6. D.E. Anagnostou, J. Papapolymerou, M.M. Tentzeris, and C.G. Christodoulou, A printed log-periodic Koch-dipole array (LPKDA), IEEE Antennas Wireless Propag Lett 7 (2008), 456–460.
7. A.A. Gheethan and D.E. Anagnostou, Reduced size planar log-periodic dipole arrays (LPDAs) using rectangular meander line elements, Proceedings Antennas Propagation Society International Symposium, San Diego, CA, 2008, pp. 1–4.
8. J. Yeo and J.-I. Lee, Planar log-periodic bow-tie dipole array antenna with reduced size and enhanced front-back ratio, Microwave Opt Technol Lett 54 (2012), 1435–1441.
9. J. Yeo and J.-I. Lee, Broadband series-fed two dipole array antenna with an integrated balun for mobile communication applications, Microwave Opt Technol Lett 54 (2012), 2166–2168.

GRAPHENE IN LAYERED MEDIUM APPLICATIONS

Ergun Simsek
Department of Electrical and Computer Engineering, The George Washington University, Washington, DC 20052; Corresponding author: simsek@gwu.edu

Received 7 February 2013

ABSTRACT: *Graphene can be defined either as an infinitely thin material with an optical conductivity or as a thin layer with a finite thickness and an effective complex electrical permittivity. Layered medium Green's functions are calculated according to these two definitions for multilayered structures including a graphene layer. It is found that numerical methods show a good agreement especially in the far field. Moreover, finite thickness method requires significantly less computation time than the effective complex permittivity method. Thus, considering the computation time and accuracy, the finite thickness approach is a better alternative to analyze the electromagnetic wave propagation and scattering in multilayered media with a graphene layer.* © 2013 Wiley Periodicals, Inc. Microwave Opt Technol Lett 55:2293–2296, 2013; View this article online at wileyonlinelibrary.com. DOI 10.1002/mop.27838

Key words: *Graphene; multilayered media; Green's functions; optical conductivity*

1. INTRODUCTION

Graphene has gathered a strong interest both from the research community and industry in the last few years because of its unique electrical and mechanical properties [1–10]. It has already found different roles in a wide range of applications including optical modulators [3], transistors [4], p-n junctions [5], sensors [6], waveguides [7], transformation optics [8], LEDs, photodetectors, absorbers, frequency converters, and many other subjects [9].

Although the interest on graphene is enormous, there are only a limited number of efforts from the computational electromagnetic (CEM) community. One of the main reasons behind this lack of response is the use of two-dimensional (2D) optical conductivity to represent this one atom thick material. Such material modeling requires a special boundary condition wherever the graphene layer is present. Alternatively, 2D optical conductivity can be converted to an effective complex electrical permittivity (ϵ_{eff}) and graphene can be treated as a 3D material with ϵ_{eff} and a finite thickness, as it is done in [7]. These two approaches are labeled as 2D and 3D, respectively, in the rest of the article.

When we examine the graphene based devices under development [1–9], we realize that most of these structures are miniaturized versions of typical mutlilayered medium applications that have been designed and analyzed by several CEM research groups for decades. Extensive research has been done to analyze electromagnetic wave propagation through and scattering from objects embedded in a multilayered medium [11–14]. One of the most commonly implemented methods is formulating the problem using layered medium Green's functions (LMGFs), so that the inhomogeneous background is not included in the solution domain (mesh) [11–14]. The particular interest of this work is the evaluation of LMGFs for a multilayered background including a graphene layer.

Two of the few studies on Green's functions and graphene are done by Nikitin et al. [15] and Hanson [16]. The former presents an analytical expression for the electromagnetic dyadic Greens function for 2D sheets including graphene [15], where the background is a homogeneous dielectric. The latter finds an exact solution for the electromagnetic field due to an electric current in the presence of a surface conductivity model of graphene [16]. However, the main focus of [16] is the surface wave propagation along graphene rather than the evaluation of LMGFs.

This work first briefly explains a mathematical model to calculate the optical conductivity of graphene as a function of angular frequency (ω), temperature (T), chemical potential (μ_c), and hopping parameter (t). Next, the modified sets of Fresnel reflection coefficients are provided to calculate LMGFs for a multilayered medium including a graphene layer, which is defined with its optical conductivity without a physical thickness. In the "Numerical Results" section, LMGFs are calculated with modified and regular Fresnel coefficients, where the effective complex permittivity approach is used for the latter. Numerical results obtained with these two different formulations are in very good agreement, especially in the far field. The effective complex permittivity approach is disadvantageous because it requires more computation time due to additional oscillations existing in the Sommerfeld integrals.

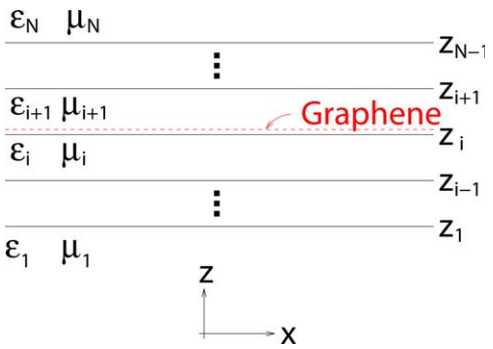

Figure 1 An N-layer medium with a graphene layer on top of the ith interface. [Color figure can be viewed in the online issue, which is available at wileyonlinelibrary.com]

2. FORMULATION

The optical conductivity of graphene can be written as $\sigma_c=\sigma_r+j\sigma_i$, where the real and imaginary parts can be calculated by using procedure found in [10]

$$\sigma_r=\sigma_0\left[\frac{18-(\hbar\omega/t)^2}{\pi 12\sqrt{(3)}}\right]\psi_r\kappa, \tag{1}$$

where

$$\psi_r=\tanh\left(\frac{\hbar\omega+2\mu_c}{4k_BT}\right)+\tanh\left(\frac{\hbar\omega-2\mu_c}{4k_BT}\right), \tag{2}$$

$$\kappa=\begin{cases}\dfrac{1}{\sqrt{F(\hbar\omega/2t)}}\mathbf{K}\left(\dfrac{2\hbar\omega/t}{F(\hbar\omega/2t)}\right), & \hbar\omega<2t\\ \dfrac{1}{\sqrt{2\hbar\omega/t}}\mathbf{K}\left(\dfrac{F(\hbar\omega/2t)}{2\hbar\omega/t}\right), & \hbar\omega\geq 2t\end{cases} \tag{3}$$

$$F(x)=(1+x)^2-025\left(x^2-1\right)^2, \tag{4}$$

$$\mathbf{K}(m)=\int_0^1\left(\left(1-x^2\right)\left(1-mx^2\right)\right)^{-1/2}dx, \tag{5}$$

and

$$\sigma_i=\frac{\sigma_0}{\pi}\left\{\Upsilon\left[1-\left(\frac{\hbar\omega}{6t}\right)^2\right]-\frac{4\mu_c}{\hbar\omega}\left[1-2\left(\frac{\mu_c}{3t}\right)^2\right]\right\}, \tag{6}$$

where

$$\Upsilon=\log\frac{|\hbar\omega+2\mu_c|}{|\hbar\omega-2\mu_c|}, \tag{7}$$

and $\sigma_0=\pi e^2/2h$, h and $\hbar$ are regular and reduced Planck constants, respectively, and k_B is Boltzmann constant. Note that the above formulation assumes a positive chemical potential. For a negative chemical potential, one can use $\sigma(\mu_c)=\sigma(-\mu_c)$.

Now consider a general multilayer medium consisting of N layers separated by $N-1$ planar interfaces parallel to the xy plane, as shown in Figure 1. Layer i exists between z_i and z_{i-1} and is characterized by relative electrical permittivity ϵ_i and relative magnetic permeability μ_i. The top surface of the ith interface is coated with graphene.

In a layered medium, electric and magnetic fields due to arbitrary electric and magnetic currents can be expressed in a dyadic form. For example, $\tilde{\tilde{\mathbf{G}}}^{EJ}(\mathbf{r},\mathbf{r}')$ is the dyadic LMGF relating electric field intensity at $\mathbf{r}$ due to electric current at $\mathbf{r}'$ [12]

$$\tilde{\tilde{\mathbf{G}}}^{EJ}(\mathbf{r},\mathbf{r}')=\begin{bmatrix} G_{xx}^{EJ} & G_{xy}^{EJ} & G_{xz}^{EJ} \\ G_{yx}^{EJ} & G_{yy}^{EJ} & G_{yz}^{EJ} \\ G_{zx}^{EJ} & G_{zy}^{EJ} & G_{zz}^{EJ} \end{bmatrix} \tag{8}$$

where $G_{\eta\zeta}^{EJ}$ gives $\hat{\eta}$ component of the electric field at $\mathbf{r}$ due to a $\hat{\zeta}$ directed unit electric dipole located at $\mathbf{r}'$, where η and ζ are either x, y, or z.

Once the dyadic LMGFs are calculated for a layered medium, the electric and magnetic fields at any point can be obtained with the superposition principle. For the details of the derivation procedure of the multilayer media Green's functions, the reader may refer to [11–14]. Briefly, first the problem domain is transformed from spatial to spectral, in which each layer is represented by a uniform transmission line having the same physical properties; hence the electric and magnetic fields can be interpreted as voltage and current, respectively, on a transmission line. Second, Green's functions in the spectral domain, called transmission line Green's functions (TLGFs), are derived by using this transmission line analogy [11,12]. Finally, TLGFs are converted to spatial domain Green's functions via proper integrations, which are as Sommerfeld integrals.

The Fresnel reflection coefficients are the main components for the evaluation of TLGFs. For a multilayered structure without a graphene layer, the reflection coefficients for TM and TE waves from the interface between the layer i and layer i + 1 can be calculated by using

$$R_{\mathrm{i,i+1}}^{\mathrm{TM}}=\frac{\epsilon_{\mathrm{i+1}}k_{z,i}-\epsilon_{\mathrm{i}}k_{z,\mathrm{i+1}}}{\epsilon_{\mathrm{i+1}}k_{z,\mathrm{i}}+\epsilon_{i}k_{z,\mathrm{i+1}}}, \tag{9}$$

$$R_{\mathrm{i,i+1}}^{\mathrm{TE}}=\frac{\mu_{\mathrm{i+1}}k_{z,\mathrm{i}}-\mu_{\mathrm{i}}k_{z,\mathrm{i+1}}}{\mu_{\mathrm{i+1}}k_{z,\mathrm{i}}+\mu_{\mathrm{i}}k_{z,\mathrm{i+1}}}, \tag{10}$$

respectively, where $k_{z,\mathrm{i}}^2=k_{\mathrm{i}}^2-k_\rho^2$, k_i is the wave-number of layer i, k_ρ is the radial wave-number (integration variable of the Sommerfeld integrals). However, if this interface is coated with graphene, then the Fresnel coefficients should be modified as follows

$$R_{\mathrm{i,i+1}}^{\mathrm{TM}}=\frac{\epsilon_{\mathrm{i+1}}k_{z,i}-\epsilon_{\mathrm{i}}k_{z,\mathrm{i+1}}-jk_{z,\mathrm{i}}k_{z,\mathrm{i+1}}\sigma_{\mathrm{c}}/\omega}{\epsilon_{\mathrm{i+1}}k_{z,i}+\epsilon_{\mathrm{i}}k_{z,\mathrm{i+1}}-jk_{z,\mathrm{i}}k_{z,\mathrm{i+1}}\sigma_{\mathrm{c}}/\omega}, \tag{11}$$

$$R_{\mathrm{i,i+1}}^{\mathrm{TE}}=\frac{\mu_{\mathrm{i+1}}k_{z,\mathrm{i}}-\mu_{\mathrm{i}}k_{z,\mathrm{i+1}}-j\sigma_{\mathrm{c}}\omega}{\mu_{\mathrm{i+1}}k_{z,\mathrm{i}}+\mu_{\mathrm{i}}k_{z,\mathrm{i+1}}+j\sigma_{\mathrm{c}}\omega}. \tag{12}$$

These slightly modified Fresnel coefficients are sufficient enough to add the capability of handling structures with graphene in any layered medium solver. However, if it is not possible to change the numerical solver algorithm (i.e., for commercial CEM solvers), then one might consider using the effective electrical permittivity approach, in which the optical conductivity of graphene is converted to a complex effective electrical permittivity by using

$$\epsilon_{\mathrm{eff}}=1-j\frac{\sigma_{\mathrm{c}}}{\omega\epsilon_0 d} \tag{13}$$

and treating graphene as a 3D material with a finite thickness d, which is equal to 0.335 nm. Again, we label the evaluation of LMGFs with modified and regular Fresnel coefficients as 2D and 3D approaches, respectively, due to the treatment of graphene. The 3D approach is an approximate solution of the 2D approach. In the next section, the accuracy of the approximate approach is examined.

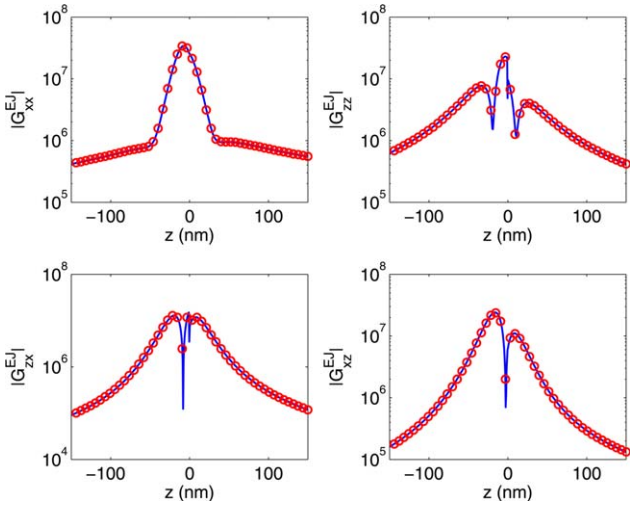

Figure 2 The magnitude of Green functions (xx, zz, zx, and xz components) for $x=25$ nm, $y=0$, $-150\ \mathrm{nm} < z < 150\ \mathrm{nm}$, $f=7.5\times10^{14}$ Hz. The source is located at (0, 0, 5) nm. Red circles and solid lines represent 2D and 3D approaches, respectively. [Color figure can be viewed in the online issue, which is available at wileyonlinelibrary.com]

3. NUMERICAL RESULTS

For the sake of simplicity, LMGF samples are calculated for an oscillating electrical dipole placed on top of a graphene coated glass slide with the relative permittivity of 2.25 and a thickness of 2 mm. The top and bottom layers are air with the relative permittivity of 1. σ_{c} is calculated for t=2.7 eV, μ_{c}=0.2 eV, and T=300 K.

Figure 2 shows the x and z components of the electric field intensity due to x and z directed electric dipoles oscillating at $f=7.5\times10^{14}$ Hz. The source is located at (0, 0, 5) nm and testing points are sampled along $-150\mathrm{nm} < z < 150\mathrm{nm}$ for x=25 nm, y=0. Eqs. (1–7) yield $\sigma_{\mathrm{c}}=613-j0055\mu\mathrm{S}$ and this value is converted to $\epsilon_{\mathrm{eff}}=10395-j43857$ for the 3D approach using Eq. (13). The results obtained with 2D and 3D approaches are in good agreement, where the maximum absolute error is 4.6%.

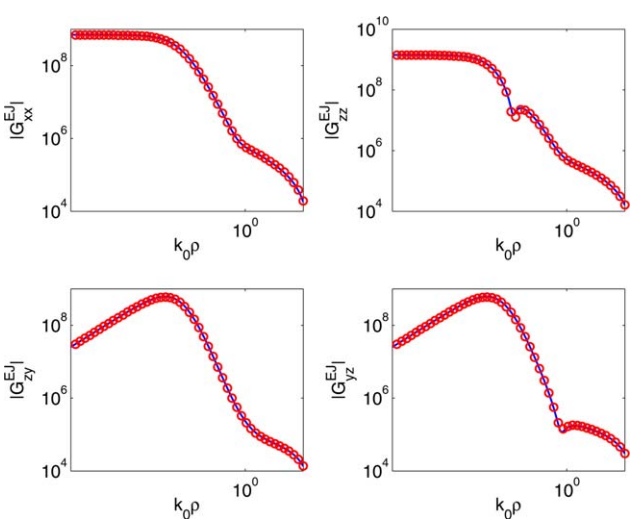

Figure 3 The magnitude of Green functions (xx, zz, zy, and yz components) for $x=0$ nm, $10^{-3} < k_0 y < 10$, $z=-5$ nm, $f=4\times10^{14}$ Hz. The source is located at (0, 0, 5) nm. Red circles and solid lines represent 2D and 3D approaches, respectively. [Color figure can be viewed in the online issue, which is available at wileyonlinelibrary.com]

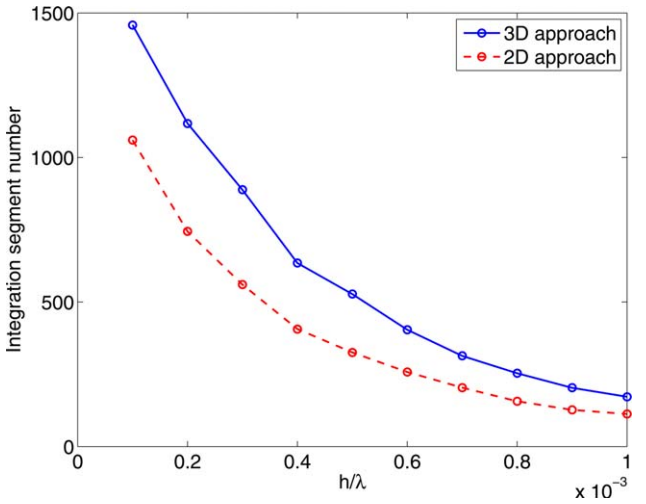

Figure 4 Number of integration segments used in adaptive integration with 3D and 2D approaches for $z'=-z=h$

For the second set of numerical results (Fig. 3), LMGFs are calculated on a horizontal line of $10^{-3} < yk_0 < 10$ for $x = 0$ nm and $z = -5$ nm at $f = 4\times10^{14}$ Hz, where $\sigma_c = 6127 - j194\ \mu$S and $\epsilon_{\text{eff}} = 126 - j82188$. The results obtained with 2D and 3D approaches are in good agreement, where the maximum absolute error is 4.2%.

Finally, we compare the number of integration segments used in adaptive integration with 3D and 2D approaches as a function of h (Fig. 4), the distance between source/test point and the interface such that $z'=-z=h$. For a fixed accuracy level, we observe that both approaches require more integration segment and hence more CPU time as the source and field points get closer to the interface. However, this increase is more significant for the 3D case as expected because of additional oscillations in the Sommerfeld integrand created by the extremely thin layer of graphene with respect to the wavelength.

4. CONCLUSION

LMGFs are calculated for multilayered structures including a graphene layer with two different approaches. For the first approach, the graphene is assumed to be infinitely thin and defined with its optical conductivity. For the second approach, an effective electrical permittivity is used to define graphene which has a thickness of 0.335 nm. Results obtained with these two approaches agree well with each other in the far field. For the near field, the maximum error is less than 5%. However, effective electrical permittivity approach might require as high as 50 percent more computation time for near-field calculations due to additional oscillations in the Sommerfeld integrands.

REFERENCES

1. K.S. Novoselov, A.K. Geim, S.V. Morozov, D. Jiang, Y. Zhang, S.V. Dubonos, I.V. Grigorieva, and A.A. Firsov, Electric field effect in atomically thin carbon films, Science 306 (2004), 666–669.
2. A.K. Geim and K.S. Novoselov, The rise of graphene, Nat Mater 6 (2007), 183–191.
3. M. Liu, X. Yin, E. Ulin-Avila, B. Geng, T. Zentgraf, L. Ju, F. Wang, and X. Zhang, A graphene-based broadband optical modulator, Nature 474 (2011), 64–67.
4. F. Schwierz, Graphene transistors, Nat Nanotechnol 5 (2010), 487–496.
5. V.V. Cheianov, V. Falko, B.L. Altshuler, The focusing of electron flow and a Veselago lens in graphene p-n junctions, Science 315 (2007), 1252–1255.
6. L. Wu, H.S. Chu, W.S. Koh, and E.P. Li, Highly sensitive graphene biosensors based on surface plasmon resonance, Opt Express 18 (2010), 14395–14400.
7. Z. Lu and W. Zhao, Nanoscale electro-optic modulators based on graphene-slot waveguides, J Opt Soc Am B 29 (2012), 1490–1496.
8. A. Vakil and N. Engheta, Transformation optics using Graphene, Science 332 (2011), 1291–1294.
9. F. Bonaccorso, Z. Sun, T. Hasan, and A. Ferrari, Graphene photonics and optoelectronics, Nat Photon 4 (2010), 611–622.
10. T. Stauber, N.M.R. Peres, and A.K. Geim, Optical conductivity of graphene in the visible region of the spectrum, Phys Rev B 78 (2008), 085432–085438.
11. W.C. Chew, Waves and Fields in Inhomogeneous Media, IEEE Press, Piscataway, NJ, 1995.
12. K.A. Michalski and J.R. Mosig, Multilayered media Green's functions in integral equation formulations, IEEE Trans Antennas Propag 45 (1997), 508–519.
13. P. Ylä-Oijala, M. Taskinen, and J. Sarvas, Multilayered media Green's Functions for MPIE with general electric and magnetic sources by the Hertz potential approach, Prog Electromagn Res 33 (2011), 141–165.
14. E. Simsek, Q.H. Liu, and B. Wei, Singularity subtraction for evaluation of Green's functions for multilayer media, IEEE Trans Microwave Theory Tech 54 (2006), 216–225.
15. A.Y. Nikitin, F.J. Garcia-Vidal, and L. Martin-Moreno, Analytical expressions for the Electromagnetic Dyadic Green's Function in Graphene and thin layers, IEEE J Selected Top Quantum Electron, in press.
16. G.W. Hanson, Dyadic Greens functions and guided surface waves for a surface conductivity model of graphene, J Appl Phys 103 (2008), 064302–064308.

A 3.1–10.6-GHz CURRENT-REUSED CMOS ULTRA-WIDEBAND LOW-NOISE AMPLIFIER USING SELF-FORWARD BODY BIAS AND FORWARD COMBINING TECHNIQUES

Chia-Hsing Wu, Yo-Sheng Lin, and Chien-Chin Wang
Department of Electrical Engineering, National Chi Nan University, Puli, Taiwan 545, Republic of China; Corresponding author: stephenlin@ncnu.edu.tw

Received 13 February 2013

ABSTRACT: *A 3.1–10.6-GHz ultra-wideband low-noise amplifier (UWB LNA) with excellent phase linearity property (group-delay variation is only ±19.46 ps across the whole band) using standard 0.18-μm CMOS technology is reported. Current reused, self-forward body bias and forward combining techniques are used to achieve low power and high-power gain (S_{21}). Both high and flat S_{21} and low and flat noise figure (NF) frequency responses are achieved by tuning the pole frequencies and pole quality factors of the second-order gain and NF frequency responses to approximate the maximally flat condition simultaneously. The LNA dissipates 6.93-mW power and achieves NF of 3.76 at 10 GHz. In addition, the LNA achieves input return loss (S_{11}) smaller than −10.6 dB, and high and flat S_{21} of 11.02 ± 0.47 dB over the 3.1–10.6-GHz band. The corresponding figure of merit (FOM) is 3.11 GHz/mW, one of the lowest FOMs ever reported for a 3.1–10.6 GHz CMOS UWB LNA. The measured input third-order intermodulation point (IIP3) is −3.6 dBm at 6 GHz.* © 2013 Wiley Periodicals, Inc. Microwave Opt Technol Lett 55:2296–2302, 2013; View this article online at wileyonlinelibrary.com. DOI 10.1002/mop.27834

Key words: *CMOS; ultra-wideband; low-noise amplifier; current reused; low power; high gain; self-forward body bias; forward combining technique*